AN ABSTRACT OF THE THESIS OF

Zhenqiu Hong for the degree of Master of Science in Forest Products presented on September 18, 1995

Title: The Measurement of Interphase Properties in Wood-Polystyrene Composites Utilizing Inverse Gas Chromatography

Signature redacted for privacy.

Abstract approved: John Simonsen

Inverse Gas Chromatography (IGC) was used to study the interphase in the wood-polystyrene composites. Thermomechanical pulp (TMP) and Douglas fir T14 fibers were progressively coated with polystyrene (PS) matrix which serve as models for the interphases. From the retention time of n-alkanes, the glass transition temperatures (T_g) of TMP-PS composites were estimated. The London (dispersive) component of surface free energies (γ^L_s) and other thermodynamic parameters on the partially coated wood fibers were determined. The plots of γ^L_s versus the polymer loadings were established. The change in the surface free energy (γ^L_s) is noted as the PS layer builds toward the pure matrix phase. The relation of γ^L_s and T_g to polymer loadings provides information on the interfacial properties of wood-polystyrene composites. It is shown that the effect of the interphase on surface properties becomes insignificant when

the polymer loading reaches ca. 12% of weight of the wood fiber substrates.

THE MEASUREMENT OF INTERPHASE PROPERTIES IN WOOD-POLYSTYRENE COMPOSITES UTILIZING INVERSE GAS CHROMATOGRAPHY

by

Zhenqiu Hong

A THESIS

submitted to

Oregon State University

in partial fulfillment of

the requirements for the

degree of

Master of Science

Completed September 18, 1995

Commencement June 1996

Master of Science thesis of Zhenqiu Hong presented on

September 18, 1995

APPROVED:

Signature redacted for privacy.

Major Professor, Representing Forest Products

Signature redacted for privacy.

Chair of Department of Forest Products

Signature redacted for privacy.

Dean of Graduate School

I understand that my thesis will become part of the permanent collection of Oregon State University libraries. My signature below authorizes release of my thesis to any reader upon request.

Signature redacted for privacy.

Zhenqiu Hong, Author

ACKNOWLEDGEMENTS

Acknowledgements are made to Dr. John Simonsen, Dr. Tim Rials, Dr. Joe Karchesy, Dr. Michael W. Schuyler and Dr. Everett M. Hansen for their valuable guidance, criticisms and suggestions. Special thanks are due to Dr. John Simonsen for his invaluable support throughout the course of study. The author extends his appreciation to Dr. Keith Levine, Dr. Gregory Rorrer, Mr. Tzu-Yang Hsien and Dr. Philip Watson for their assistance during the study. Finally, the author wish to express his appreciation to his wife, Yanrong Wang, for her patience and encouragement.

TABLE OF CONTENTS

Page

1. INTRODUCTION 1

    1.1 Wood-Plastic Composites 1

    1.2 Wood-Plastic Interphase 2

2. LITERATURE REVIEW 4

    2.1 Wood-Plastic Composites 4

    2.2 Wood-Polystyrene Composites 6

    2.3 Inverse Gas Chromatography. 8

        2.3.1 General introduction 8

        2.3.2 Interaction of probe and stationary phase . .9

        2.3.3 IGC instrumentation 10

        2.3.4 Zero coverage 12

        2.3.5 IGC retention diagram 13

        2.3.6 Thermodynamic functions 15

3. OBJECTIVES 21

4. MATERIALS AND METHODS 22

    4.1 Wood Fibers 22

    4.2 Polystyrene 23

    4.3 N-Alkane Probes 23

    4.4 Column Preparation 23

    4.5 IGC Measurements 24

5. RESULTS AND CONCLUSION 27

    5.1 Retention Behavior of N-Alkane Probes. 27

    5.2 Thermodynamics of Adsorption. 35

TABLE OF CONTENTS (Continued)

Page

5.2.1 Standard free energy of adsorption 35

5.3.2 Standard enthalpy of adsorption 36

5.3.3 Standard entropy of adsorption 44

5.3.4 London component of surface free energy . . 44

6. CONCLUSIONS 57

7. LITERATURE CITED 59

LIST OF FIGURES

Figure **Page**

1. Wood-plastic interphase 2

2. A schematic for IGC apparatus 11

3. A typical chromatogram of IGC 11

4. Retention diagram for an amorphous polymer 16

5. Retention variation with probe size for TMP-PS* samples at 70^0C 28

6. Retention variation with probe size for CW-PS samples at 60^0C 29

7. Ln V^0_g versus 1/T for CW-4%PS 30

8. Ln V^0_g versus 1/T for T14-8%PS 31

9. Retention diagram ln V^0_g versus 1/T of n-decane TMP-PS* samples 34

10. Linear variation of ΔG^0_A with probe size for TMP-PS* samples at 60^0C 38

11. Linear variation of ΔG^0_A with probe size for CW-PS samples at 60^0C 39

12. Linear variation of ΔG^0_A with probe size for T14-PS samples at 60^0C 40

13. Variation of ΔH^0_A with probe size for TMP-PS* Samples 42

14. London component of free energy for CW-PS samples. .53

15. London component of free energy for TMP-PS* samples 54

16. London component of free energy for T14-PS samples. .55

17. London component of free energy for White pine at 60^0C 56

LIST OF TABLES

Table		Page
1.	Column parameters of TMP-PS* samples	26
2.	Column parameters of CW-PS samples	26
3.	Column parameters of CW-PS samples	26
4.	Estimated T_g from IGC	33
5.	Standard free energy ΔG^0_A at 60^0C	37
6.	Standard enthalpy of adsorption ΔH^0_A at 60^0C	43
7.	Standard thermodynamic functions for adsorption of $C_{10}H_{22}$ at 60^0C	45
8.	Standard entropy of adsorption ΔS^0_A at 60^0C	46
9.	London component of free energy γ^L_S for the three substrates at 60 and 70^0C	49

THE MEASUREMENT OF INTERPHASE PROPERTIES IN WOOD-POLYSTYRENE COMPOSITES UTILIZING INVERSE GAS CHROMATOGRAPHY

1. INTRODUCTION

1.1 Wood-Plastic Composites

The term "wood-plastic composites" denotes materials formed from mixtures of wood and plastics. The wood component can be in the form of either fibers or particles. The main types of plastics are thermoplastics and thermosets. The former melt when heated and solidify upon cooling and thus are recyclable. The latter, however, are cross-linked between polymer molecular chains and therefore difficult or impossible to reformulate. Many different types of wood and plastic may be used to manufacture these composites. Since wood contains cellulose, hemicellulose, lignin and other low molecular weight chemical compounds, wood fibers are hydrophilic. Most synthetic plastics, however, are hydrophobic. In comparison to wood, most plastics are resistant to rot and stable with respect to moisture (1).

1.2 Wood-Plastic Interphase

A fiber reinforced plastic can be considered to consist of three phases: the bulk plastic matrix, the wood fiber phase and the interface or interphase between the two. The terms interface and interphase are used interchangeably in the literature. **Figure 1** depicts a schematic of a wood-plastic interphase.

The wood fiber-plastic interphase can be considered to

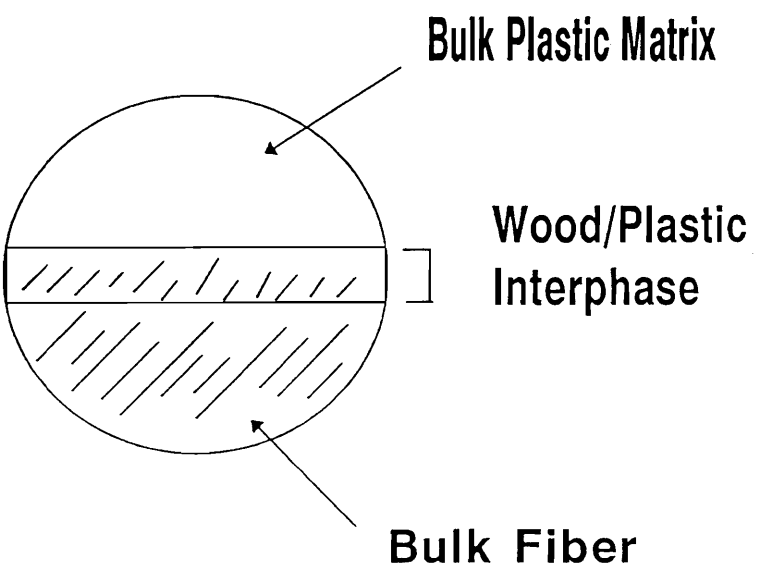

Figure 1. Wood-plastic interphase.

be a third constituent of a composite material. The interfacial bonding between wood fiber and plastic might include mechanical, covalent, ionic, hydrogen bonding and Van der Waals forces. The Van der Waals force includes dipole-dipole interactions, induced dipole interactions, and London dispersion forces. The strength of the interphase depends on the extent of bonding between the matrix and the filler.

In order for the fibers to act as reinforcements, stresses applied to the matrix must be transferred across the interface region to the stiffer fibers. Under stress, a poor interface will result in pulling out of the fibers from the plastic matrix and consequently failure of the composite. Since the efficiency of stress transfer from the matrix to the fiber depends upon the interfacial bonding, the properties of the composite, especially the ultimate properties, are largely determined by the interface. The quality of the interphase is so important that it may govern the final performance of a given wood fiber-plastic composite.

2. LITERATURE REVIEW

2.1 Wood-Plastic Composites

Wood-plastic composites have received intensive study in recent years (2,3,4,5). The advantages of light weight and low cost that are provided by lignocellulosic fibers have long been recognized in the plastics industry where these materials have been extensively used as fillers and extenders for various thermosetting polymer matrices. The early use of wood was mostly as a low-cost extender for thermosetting resins (4). Over the past few decades, attempts have been made to use wood fibers for manufacturing wood-plastic composites by using both thermosets and thermoplastic matrices. The most frequent use of thermoplastics includes polypropylene (PP), polyethylene (PE), polystyrene (PS), poly(vinyl chloride) (PVC) and polyester (3). In contrast to thermosetting plastics, wood fibers and thermoplastics are recyclable. Wood fibers are generally stronger than most thermoplastics. In combination with fiber strength and thermoplastic flexibility, composites manufactured from these materials offer many potential benefits: Low cost, ease of processing, flexible design of properties, and recyclability. After these potential benefits were recognized, research on methods to utilize wood fibers to

reinforce plastics became popular (2). The most attractive advantage of wood fiber-plastic composites made from thermoplastics is that they offer an opportunity to use recycled plastics and recycled wood (6).

Although many technological advances have been made, some problems still remain. The most notable problem that must be addressed in wood-thermoplastic polymer systems is the lack of adhesion between the two components (7,8). From the point view of chemical composition, wood fiber contains cellulose, hemicellulose, lignin and other extractive compounds. It is a hydrophilic material. Most plastics, such as polystyrene (PS), polyethylene (PE) and poly(vinyl chloride) (PVC), however, are hydrophobic materials. The different polarities of the fibers and plastics lead to incompatibility of the two components (9). As a direct result of this incompatibility, an inferior fiber-matrix interface is established that prevents the necessary stress transfer from the polymer matrix to the load bearing fiber, relegating the function of the fiber to that of a non-reinforcing filler. Typically, only a small fraction of the strength and stiffness of the fibers has been translated to the final material properties of the composites. In order to develop high quality composites, it is important to acquire a better understanding of the properties of the interface.

2.2 Wood-Polystyrene Composites

Wood-polystyrene (PS) composites, one of many wood fiber-plastic composites, have also received intensive study in recent years (8,9,10). Polystyrene (PS) is a thermoplastic. Its molecular formula is:

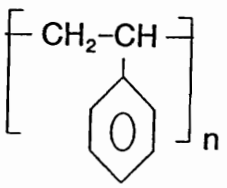

The incompatibility between wood fibers and polystyrene (PS) has also been widely recognized (2,9). Many efforts have been made to improve the strength of the interphase and the final performance of wood-polystyrene composites (2,10). The prevailing conceptual approach to compatibilization is to maximize the interfacial shear strength (11,12). There are several methods that can be used to enhance the interfacial reaction between wood fiber and polystyrene (PS). These include surface pretreatment of fiber and addition of coupling agents to the composite system. Schreiber and coworkers (13) investigated the effect of plasma modification on the properties of wood fiber-PS and other fiber-plastic composites. The techniques including IGC (Inverse Gas Chromatography), XPS (X-ray

Photoelectron Spectroscopy) and SEM (Scanning Electron Microscope) were used to evaluate the effectiveness of fiber surface treatment. It indicated that the mechanical properties of the fiber-PS composite were improved by using plasma modification. The most interesting part of the work is that the IGC technique was used to determine the fiber-PS interaction characteristics, such as the dispersion (London) surface free energy, although its emphasis was placed on the evaluation of acid/base interaction suggested by Gutmann (14).

Numerous reports indicate that coupling agents play an important role in improving mechanical properties of fiber-PS composites (8,9,10). The function of the coupling agent is to improve the compatibility and dispersibility between wood fiber and polystyrene. Maldas and Kokta (2) investigated the influence of maleic anhydride (MA) and a polymeric isocyanate as coupling agents on the performance of wood fiber-PS composites. An overall improvement in the mechanical properties was achieved due by the addition of MA or polymeric isocyanate.

While these studies have shed considerable insight into potential solutions, they have largely relied on secondary properties to evaluate composite performance rather than focus specifically on the characteristics of the interfacial region of the composite system. As such, very little information has been gained on the fundamental

physico-chemical parameters that control the structure and properties of the wood fiber-polymer matrix interface.

2.3 Inverse Gas Chromatography

2.3.1 *General introduction*

There are few experimental techniques that yield data which can be mathematically related to the properties of the interface. One such technique is inverse gas chromatography (IGC) (15). IGC is capable of characterizing the solid surface and interface properties. The general principles and applications have been reviewed in the literature (16) . The major application of IGC is in the area of polymer science and engineering. It can be used for the study of (16):

1) Sorption and diffusion in polymers;

2) Polymer blend characterization;

3) Surface and interface characterization of polymers and fiber-polymer composites .

IGC was developed on the basis of conventional gas chromatography (GC). It was invented and developed in the late 1970's (17). The instrumentation of IGC and conventional GC are similar. In IGC, a non-volatile material to be investigated is packed within a GC column. This stationary phase is then characterized by injecting known volatile chemical compounds — probes. The

interaction of gaseous probe molecules with a stationary phase results in a retention time, t_R, which then can be translated into a number of important thermodynamic parameters. The obtained thermodynamic data can be related to the surface and/or other properties of the stationary phase (18).

2.3.2 *Interaction of probe and stationary phase*

The molecular interaction and physical forces between solute (probe) and a stationary phase include :

1) Ionic interaction;

2) Hydrogen bonding;

3) Van der Waals forces.

The Van der Waals forces arise from following three types of interactions between a probe and a stationary phase (19):

1. Dipole-dipole interaction;
2. Dipole-induced dipole interaction;
3. Induced dipole-induced dipole interaction.

The physical force resulting from induced dipole-induced dipole interaction is referred to as dispersive (London) forces.

It was assumed that the surface free energy of a solid is the sum of two terms: a dispersive component γ^L_S and a non-dispersive or polar component γ^P_S (20). When a probe and a stationary phase are both nonpolar, the interaction is

primarily the induced dipole-induced dipole interaction, i.e. London (dispersive) force. In this circumstance, the London (dispersive) component of the surface free energy can be determined by using non-polar probes.

2.3.3 *IGC instrumentation*

The instrument used in IGC is similar to conventional GC. **Figure 2** presents a schematic of a gas chromatograph for IGC (21). Nitrogen or helium is typically used as the carrier gas. When the probe is injected into the injection oven, it evaporates rapidly since the temperature is higher than its boiling point. The vapor is carried by the carrier gas, and flows through the GC column packed with the solid sample of interest. As the probe travels through the stationary phase, partitioning occurs via sorption-desorption. The probe's interaction with the stationary phase will result in a retention time t_R which is monitored by the FID (Flame Ionization Detector) and recorded by an integrator.

Retention times can be normalized by injecting a marker, for example methane. The net retention time (t_N) of the probe can be obtained. A typical gas chromatogram is shown in **Figure 3.**

In the illustrated chromatogram, t_m is the retention time of marker; t_R, the retention time of probe; t_N, the net retention time of probe. From net retention time, a net

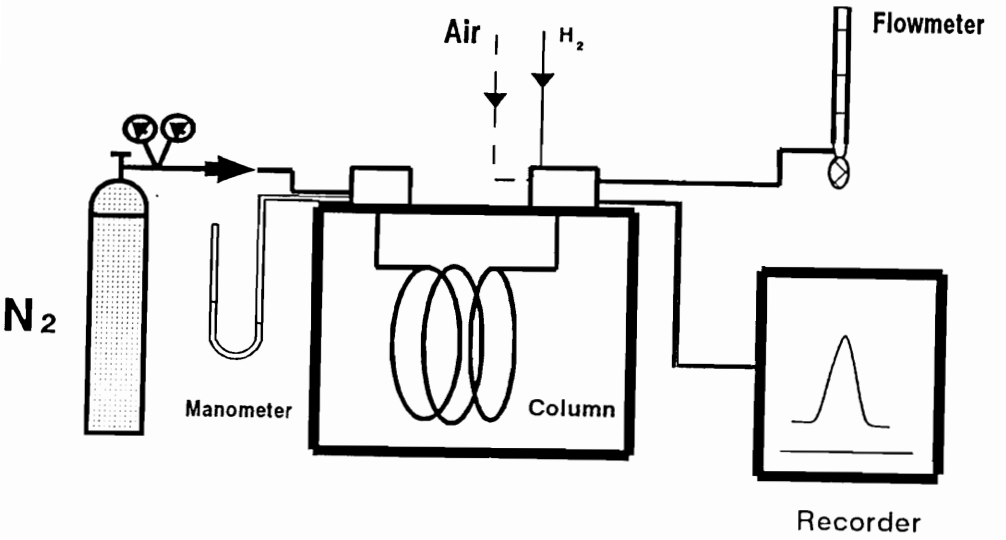

Figure 2. A schematic for IGC apparatus.

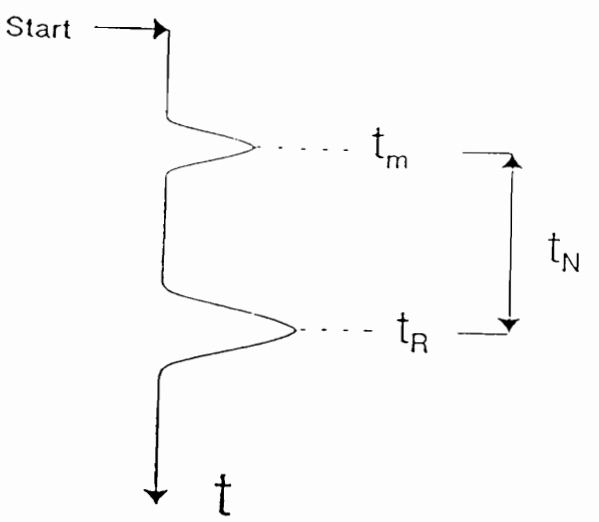

Figure 3. A typical chromatogram of IGC.

retention volume is then calculated from equation (1)(22):

$$V_N = F\, j\, (t_R - t_m) \qquad (1)$$

where F is a corrected flow rate of the carrier gas; j, a pressure-gradient correction factor for gas compressibility. The correction factor j is given by (23,24):

$$j = \frac{3}{2}\left[\frac{(P_i/P_o)^2 - 1}{(P_i/P_o)^3 - 1}\right] \qquad (2)$$

where P_i and P_o are the inlet and outlet pressures of the GC column (24).

2.3.4 *Zero coverage*

IGC has been used successfully for studying the surface properties of solids by adsorption of vapor at a gas-solid interface. Unlike conventional adsorption techniques, IGC allows the measurement of adsorption data down to low vapor concentrations where the surface coverage approaches zero, which is referred to as zero coverage. At zero coverage, adsorbate-adsorbate (probe-probe) interactions are negligible, and thermodynamic functions depend only on adsorbate-adsorbent interactions (25). IGC

has been used at zero surface coverage to characterize the surfaces of cellulose (26).

At small concentrations of the probe, the fundamental parameter measured in IGC is the retention volume, V_N, which obeys Henry's Law (26):

$$V_N = K_s A \qquad (3)$$

where K_s is the surface partition coefficient for the adsorbate (m); and A, the total surface area of adsorbent in the column (m^2).

V_N is then converted to a specific net retention volume, V^0_g, by using the following equations (27):

$$V_g^0 = \frac{273.15}{T} \times \frac{Vn}{W} \qquad (4)$$

where T is the column temperature (^0K); W, the weight of adsorbent (g).

2.3.5. *IGC retention diagram*

The retention diagram is obtained by plotting the logarithm of the specific retention volume (V^0_g) versus the reciprocal of the absolute temperature as shown in **Figure 4**. The retention diagram gives several important pieces of

information regarding transitions in the polymer stationary phase (21,28):

1) Segment AB. The polymer is below its glass transition temperature (T_g) in this temperature region . In this region retention of the probe results primarily from condensation and adsorption of the probe onto the surface of the stationary phase. Diffusion of the probe molecules into the bulk polymer phase is insignificant in this region. The retention diagram is linear and gives information on the surface properties of the stationary phase. The slope of the straight line is used to determine the enthalpy of adsorption of the probe on the solid surface (27).

2) Point B. This point corresponds to the glass transition temperature (T_g). Due to the mobility of segment polymer molecules, penetration of the probe molecule into the bulk of the polymer begins, causing an increase of the retention volume with temperature. In wood-polystyrene composites, the T_g might respond to the change of the amount of PS loading on wood fibers.

3) segment BC. In this temperature region, non-equilibrium absorption occurs due to an initially slow rate of diffusion of the probe into and out of the stationary phase.

4) Point C, This point corresponds to the equilibrium conditions of the diffusion process.

5) Segment CD. In this temperature region, equilibrium bulk absorption occurs, but polymer-probe interaction is restricted to the amorphous polymer.

6) Segment DE, In this temperature region, the fraction of the amorphous phase increase, leading to an increase in retention volume.

7) Point E. This point corresponds to the melting point temperature (T_m) of the polymer.

8) Segment EF. In this temperature region, the retention diagram is linear again as a result of the bulk sorption into the molten polymer.

In the region of line AB in Figure 4, the retention diagram is linear and its slope is related to the enthalpy of adsorption on the solid surface according to (15):

$$\frac{\partial \ln V_g^0}{\partial (1/T)} = - \frac{\Delta H^0_A}{R} \qquad (5)$$

where R is the gas constant; T, the column temperature; ΔH^0_A, the enthalpy of adsorption on the solid surface.

2.3.6 *Thermodynamic functions*

Further development of this technique has led to the determination of thermodynamic data. The thermodynamic functions of adsorption can be derived from retention

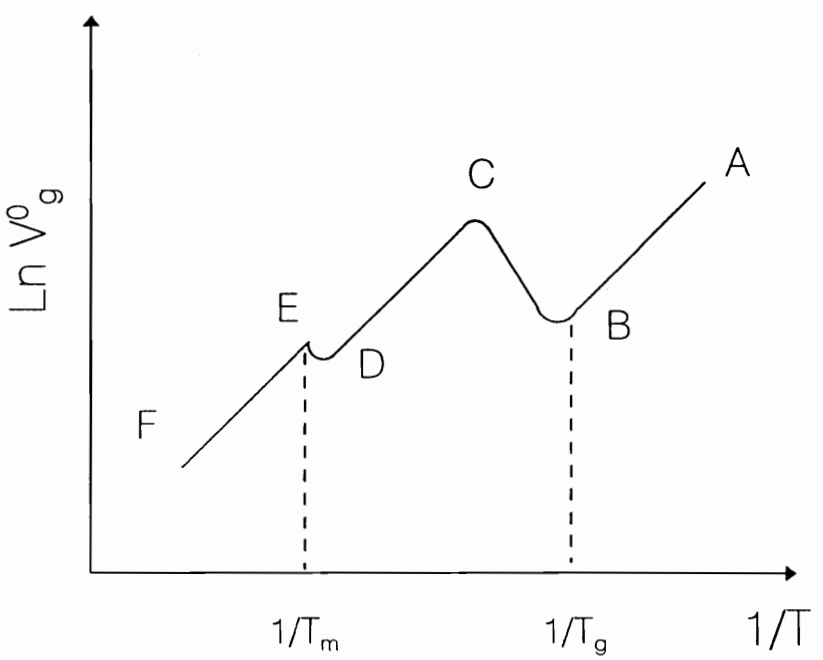

Figure 4. Retention diagram for an amorphous polymer.

volume data. The following equations (26) are used to calculate the standard free energy ΔG^0_A , which represents the standard free energy change for the isothermal adsorption of 1 mole of adsorbate from the standard gaseous state to a standard state on the surface; ΔH^0_A, the standard molar enthalpy of adsorption; ΔS^0_A, the standard entropy of adsorption; q_d, the differential heat of adsorption. At zero coverage, q_d is equal to $-\Delta H^0_A$.

$$\Delta G^0_A = -RT \ln(K_S \cdot P_{s,g}/\pi_s) \qquad (6)$$

$$\Delta H^0_A = -R \frac{d(\ln V^0_g)}{d(1/T)} \qquad (7)$$

$$\Delta S^0_A = -\frac{(q_d + \Delta G^0_A)}{T} \qquad (8)$$

where R is the gas constant (8.3143 J/K mole); T, the column temperature (^{0}K); K_s, the surface partition coefficient for the adsorbate ; $P_{s,g}$, adsorbate vapor pressure at the standard state (101 kN/m^2) ; Π_s, the reference two-dimensional surface pressure (0.038 mN/m), defined by De Boer (26).

In the case of a nonpolar liquid adhered to a solid surface, the work of adhesion can be separated into two terms (29):

$$W_A = 2(\gamma_1 \gamma^L_s)^{1/2} \qquad (10)$$

where γ_l is the surface tension of the nonpolar liquid; γ^L_s, the London component of the solid surface free energy.

Dorris and Gray (26) have extended this concept for an homologous series of alkanes. They assume W_A to be equal to the free energy of adsorption per unit area of the surface:

$$W_A = -\Delta G^0_A \; / \; N \; a_{CH2} \qquad (11)$$

where N is the Avogadro's number and a_{CH2} is the surface area occupied by an incremental n-alkane methylene group ($-CH_2-$) (0.06 nm^2). Using the known value for the surface tension of incremental methylene units, the London component of the surface free energy can be calculated from (30):

$$\gamma^L_s = \frac{1}{4\,\gamma_{CH_2}} \left[\frac{\Delta G^0_A\,(CH_2)}{N\,a_{CH_2}}\right]^2 \qquad (12)$$

where the $\Delta G^0_A\,(CH_2)$ is the free energy of adsorption of an incremental methylene group in a series of n-alkane probes and is obtained by measurement of the free energy

for an homologous series of n-alkanes. The ΔG^0_A (CH_2) is given by:

$$\Delta G^0_A(CH_2) = \frac{d\Delta G^0_A}{dn} \qquad (13)$$

where n is the number of carbon atoms in an homologous series of n-alkanes.

This IGC technique was extended to the study of cellulose fibers by Mohlin and Gray (31). Further development of this technique has led to the determination of thermodynamic data of fiber and paper surfaces. Dorris and Gray (26,32) studied paper and wood fiber surfaces by using IGC to determine the London component of surface free energies and other thermodynamic functions. Kamdem and Riedl (27) used IGC to study the surface of chemithermomechanical pulp (CTMP) fiber with methyl methacrylate (MMA) grafted onto the fiber. The thermodynamic data then were used to evaluate the fiber surface modification by polymer grafting. The authors concluded that IGC is a powerful, versatile and convenient method to study and characterize solid surfaces. Gurnaul and Gray (33) measured the standard free energy, the enthalpy, the entropy of adsorption and London component

of surface free energy of kraft paper surfaces. These thermodynamic parameters then were used to evaluate the interactions of probes and paper surfaces, and the surface properties of different papers.

3. Objectives

The objective of this study was to determine specific thermodynamic parameters of the interphase in wood-polystyrene composites using inverse gas chromatography (IGC).

4. Materials and Methods

4.1 Wood Fibers

The thermomechanical pulp (TMP) was obtained from the Smurfit Newsprint Corp. pulp mill in Newburg, Oregon. It consists primarily of Western Hemlock and a mixture of firs. The fiber was obtain from the slurry stream prior to bleaching, air dried, ground in a Wiley mill to pass a 16 mesh screen, dried in vacuo at 60^0C overnight and stored over a silica gel desiccant. The average length of the TMP fiber was found to be 1.0 mm with a standard deviation of 0.6 mm.

Wood flour from Douglas fir (Pseudotsuga menziesii (Mirb.) Franco) ground to 80-100 mesh was contributed by the Menasha Wood Corporation, Olympia, Washington as product T14. The T14 was dried in vacuo at 60^0C overnight and stored over a silica gel desiccant. This filler was analyzed optically and found to have an average length of 0.9 mm with a standard deviation of 0.6 mm. The average aspect ratio was nine with a standard deviation of five. T14 was soaked in toluene overnight, filtered and dried in vacuo at 60^0C.

4.2 Polystyrene (PS)

Two different polystyrene samples were used in this experiment: a product 685D, obtained from Dow Chemical Co. PS*; and a product 846 from Scientific Polymer Products, Inc. PS.

4.3 N-Alkane Probes

A series of normal alkanes C_8H_{18}, C_9H_{20}, $C_{10}H_{22}$, $C_{11}H_{24}$ and $C_{12}H_{26}$ were obtained from Aldrich Chemical Co. and used without further purification.

Chromosorb W (CW) of 60/80 mesh was obtained from Applied Science Laboratories, Inc. The compound was dried under vacuum at 105^0C prior to use.

4.4 Column Preparation

Polystyrene (PS*) was dissolved in HPLC grade toluene to make a 1% solution. TMP fiber was coated with PS* by mixing with the 1% solution of PS* in toluene, then allowing the solvent to evaporate. This was done several times to ensure a uniform coating and to build up the desired percent weight of PS* on TMP fiber. The PS* loadings on TMP fiber ranged from 0, 2, 4, 8, 12, to 20%, and the corresponding samples are labelled as TMP-0%PS*, TMP-2%PS*, TMP-4%PS*, TMP-8%PS*, TMP-12%PS* and TMP-20%PS*, respectively.

Same procedures were followed for coating PS on CW and T14 substrates. The PS loadings on CW and T14 were 0, 2, 4, 8 and 12%. A 20% PS loading on T14 was also made.

Standard gas chromatography (GC) Teflon tubing sections, 1/4 inch in diameter by 1 meter long were packed with the coated wood fiber or Chromosorb W (CW) samples. Each of these columns was conditioned in the GC at 60^0C for two hours with TMP samples and overnight at 105^0C for with the CW and T14 samples. **Table 1, 2** and **3** show the columns prepared.

4.5 IGC Measurements

An Hewlett-Packard 5840A equipped with a flame ionization detector (FID) was used for IGC studies. Nitrogen was used as the carrier gas and its flow rate was set at about 30 ml/min. at room temperature. The inlet pressure, P_i, of the column was measured by a mercury manometer. The outlet pressure, P_o, of the column was atmospheric pressure and was determined by a mercury manometer.

The injection port was set at 200^0C and the detector at 150^0C. Injections were made from the air space above a sample bottle (vial) of the desired probe which had been purged with methane. The injection volume was less than 0.5 μl. A series of n-alkanes were used as probes and methane as non-interacting marker. At least four injections were

made for each probe. Retention time was the mean value of four measurements.

Each column was conditioned at 105^{0}C for overnight and was equilibrated for 2 hours at the specified column temperature before measurement. The column temperatures were set at 50, 60, 70, 80, 90, 100 and 110^{0}C for TMP-PS* samples; 50, 55, 60, 65 and 70^{0}C for CW-PS and T14-PS samples.

Retention time was obtained directly from the IGC chromatogram. The specific retention volume V^0_g was determined according to equation (4). The London component of the surface free energy, γ^L_S, was determined from equation (12).

Table 1. Column parameters of TMP-PS* samples.

Column	PS* Loading(%)
TMP-0%PS*	0
TMP-2%PS*	2
TMP-4%PS*	4
TMP-8%PS*	8
TMP-12%PS*	12
TMP-20%PS*	20

Table 2. Column parameters of CW-PS samples.

Column	PS Loading(%)
CW-0%PS	0
CW-2%PS	2
CW-4%PS	4
CW-8%PS	8
CW-12%PS	12

Table 3. Column parameters of T14-PS samples.

Column	PS Loading(%)
T14-0%PS	0
T14-2%PS	2
T14-4%PS	4
T14-8%PS	8
T14-12%PS	12
T14-20%PS	20

5. RESULTS AND DISCUSSION

5.1 Retention Behavior of N-Alkane Probes

The retention times of the probes were obtained directly from IGC chromatogram. The variation of the retention times was less than 3%.

The specific retention volume V_g^0 for all stationary phases, CW-PS, TMP-PS* and T14-PS samples, was obtained according to equation (4). Plots of ln V_g^0 versus number of carbon atom of the probes were established. The results for TMP-PS* and CW-PS samples are given in **Figure 5** and **6**. The lack of the value ln V_g^0 of C_8H_{18} for TMP-20%PS* was due to extremely short retention time of C_8H_{18}. It shows the linear variation of ln V_g^0 with the probe size and the percentage of PS loading on the TMP and CW substrates. Similar results for the rest of the samples were observed. In combination with the independence of the retention time on probe injection volume, the linearity suggests there is no significant error caused by injection size or instrumental fluctuation.

In the temperature range from 50^0C to 80^0C, far below the PS glass transition temperature (T_g) of 98^0C, the plots of ln V_g^0 versus 1/T for all samples are linear. The results of CW-4%PS and T14-8%PS* are presented in **Figure 7** and **8**. The linear dependency of ln V_g^0 on the reciprocal

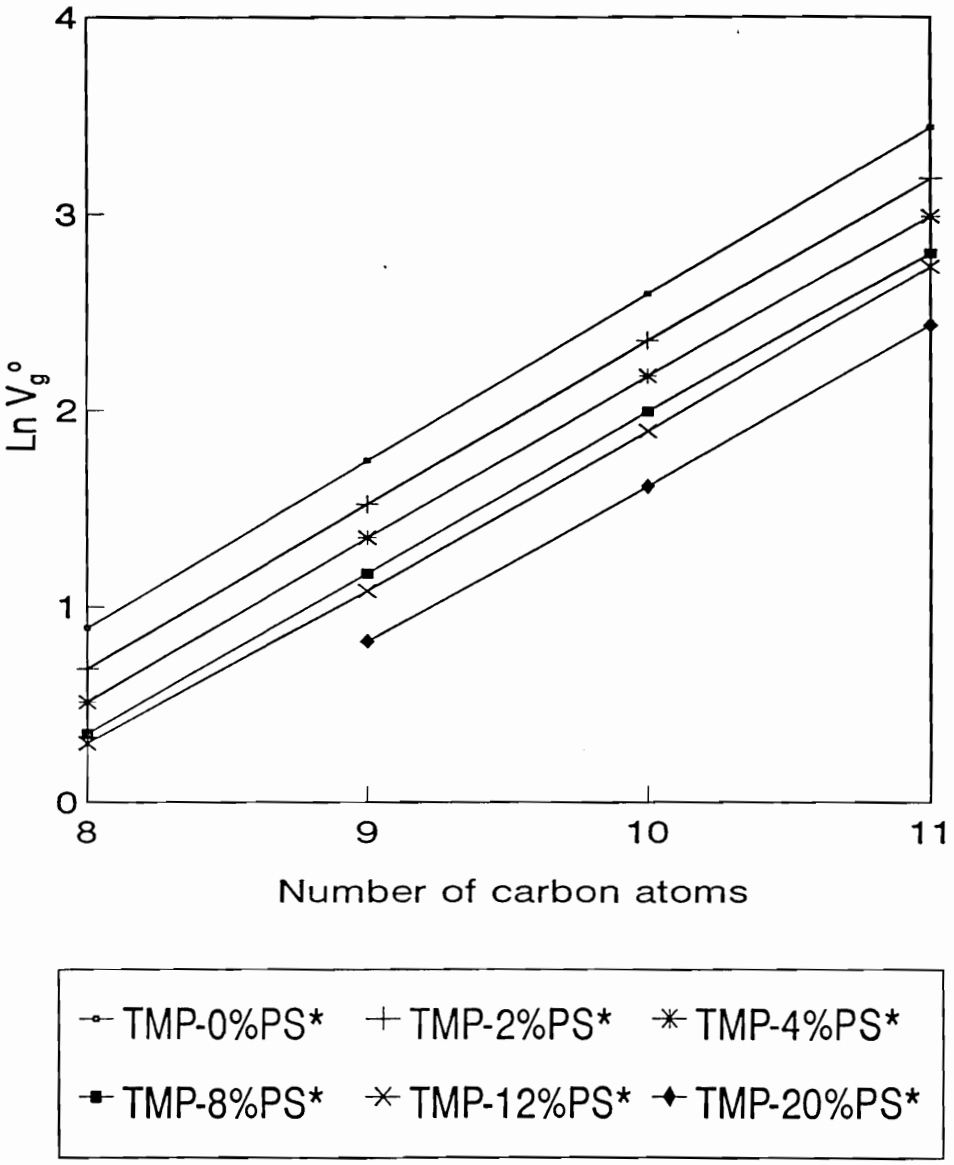

Figure 5. Retention variation with probe size for TMP-PS* samples at 70^0C.

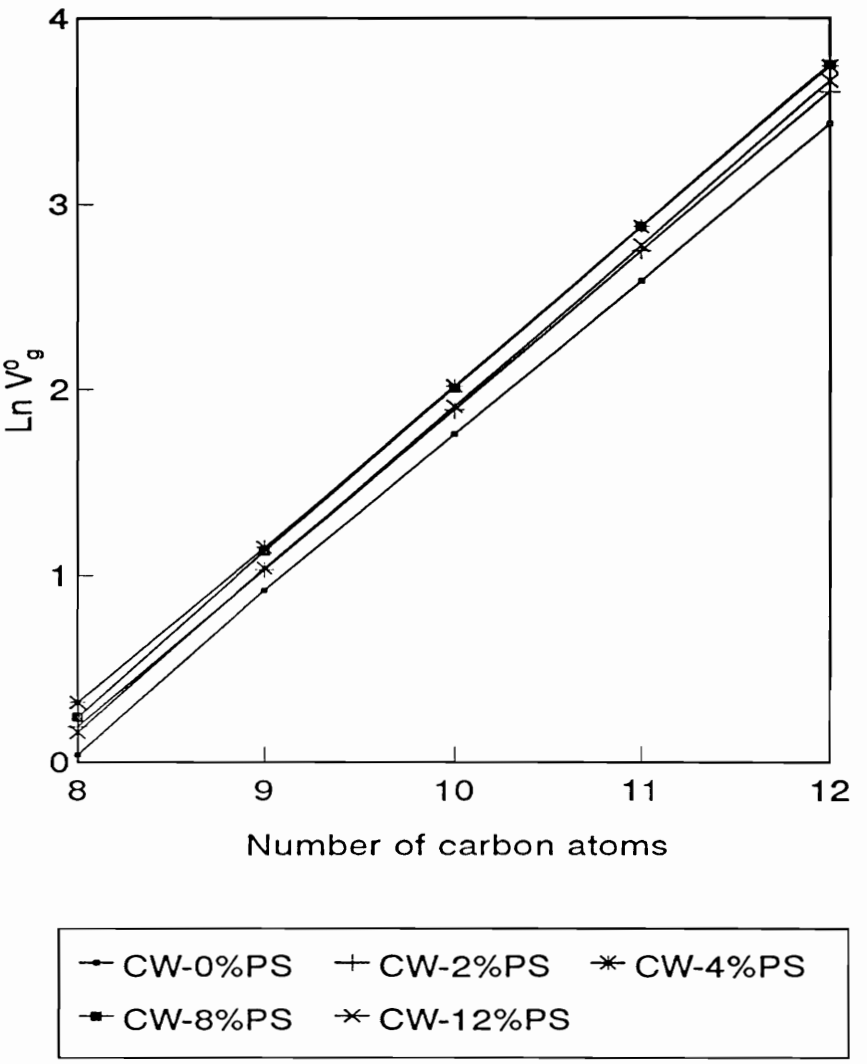

Figure 6. Retention variation with probe size for CW-PS samples at 60^0C.

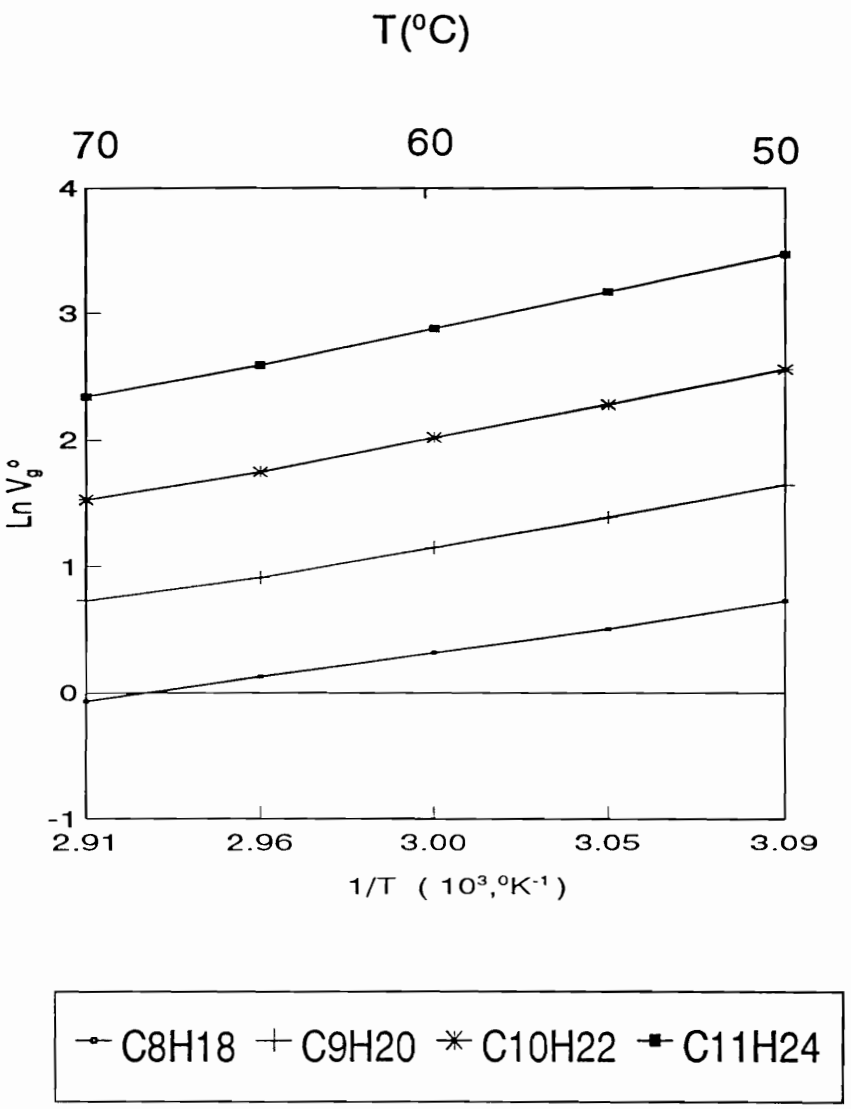

Figure 7. Ln V^0_g versus 1/T for CW-4%PS.

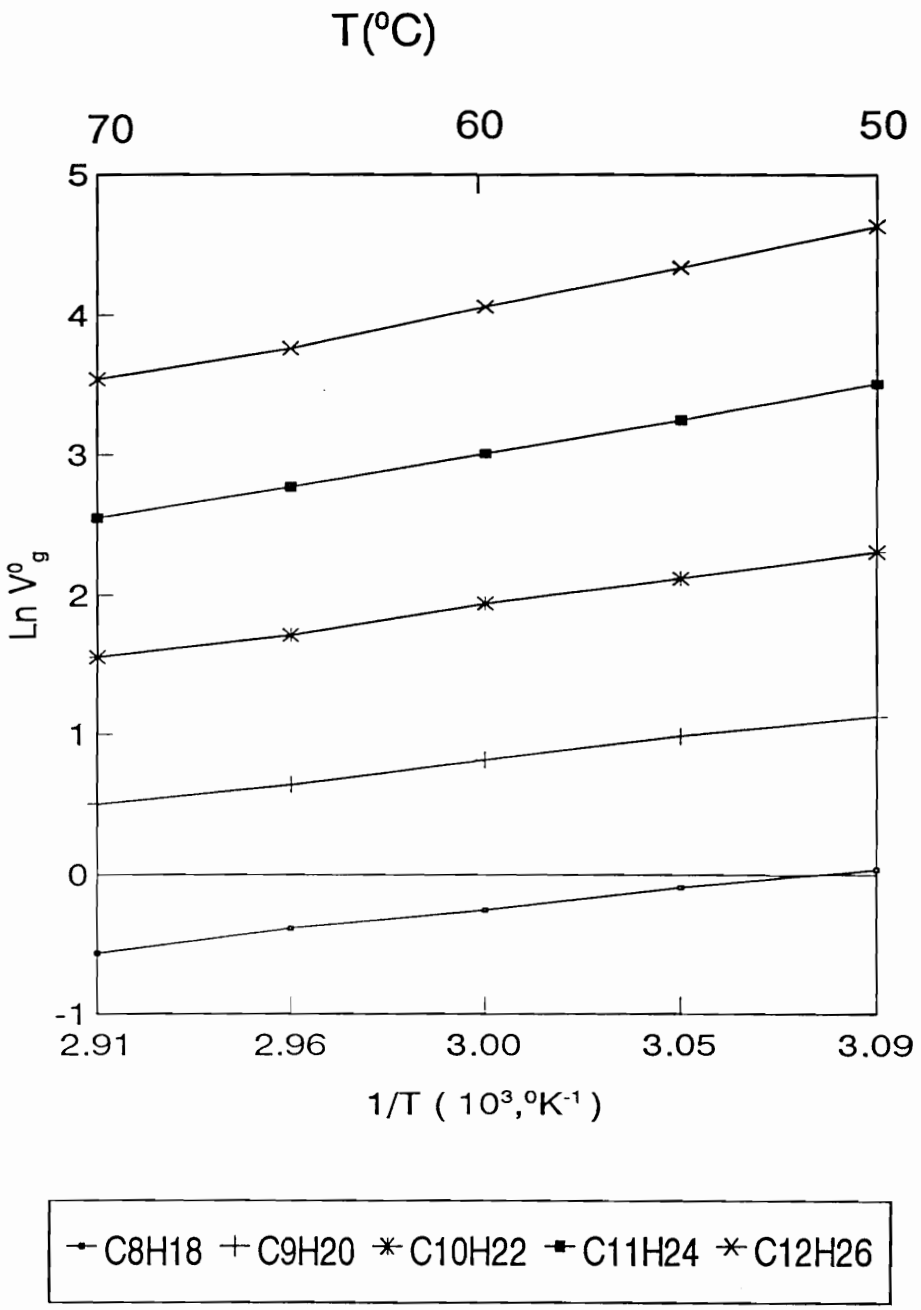

Figure 8. Ln V^0_g versus 1/T for T14-8%PS.

temperature confirms the validity of equation (7). The standard enthalpy of adsorption, ΔH_A^0, was calculated from the slope using equation (5) (27,34).

V_g^0 was also obtained for PS* on TMP at higher temperatures up to 110°C. The plot should give information on the glass transition temperature T_g (15). The retention behavior of probes will change as the temperature rises through T_g. Below the T_g, the retention time of the probe arises mainly from condensation and adsorption of the probe onto the surface of the stationary phase. V_g^0 decreases with increasing temperature. When the temperature reaches T_g, penetration of the probe molecule into the polystyrene (PS) begins, due to the mobility of segment PS molecules, resulting in an increase of the retention volume with temperature. The T_g is indicated by the deviation from linearity of the plot. The plots of ln V_g^0 versus 1/T of n-decane for TMP-PS* samples are presented in **Figure 9**. The values of ln V_g^0 for 50 to 80°C were used to construct a first order regression line. The deviation of the experiment data from this line was determined graphically. The use of IGC allows the determination of the T_g under conditions difficult to measure with other techniques. The measurement of T_g essentially requires determining the intersection of a line and tangent. This methods does not allow for precise measurement of the T_g, but does provide an estimate of the T_g in the interface of PS coated wood

fibers and Chromosorb W (CW). A linear variation of T_g with 1/T is observed for the pure TMP sample, i.e. TMP-0%PS, in **Figure 9.** When the TMP was coated with 2% PS, the departure from linearity becomes evident starting at the temperature around 80^0C. The ranges of T_g estimated from the first deviation are included in **Table 4.** Since the temperature interval for determination of T_g in this experiment was 10^0C, it did not allow for estimate the T_g accurately. If the temperature interval becomes small, however, it does allow for more accurate determination of T_g. Using the first deviation from linearity to determine of T_g for PS loading on Chromosorb G and Chromosorb AW surfaces was reported by Braun and Guilt (24).

Table 4. Estimated T_g from IGC.

Column	T_g (^{0}C)
TMP-2%PS*	80 - 90
TMP-4%PS*	80 - 90
TMP-8%PS*	80 - 90
TMP-12%PS*	80 - 90
TMP-20%PS*	80 - 90

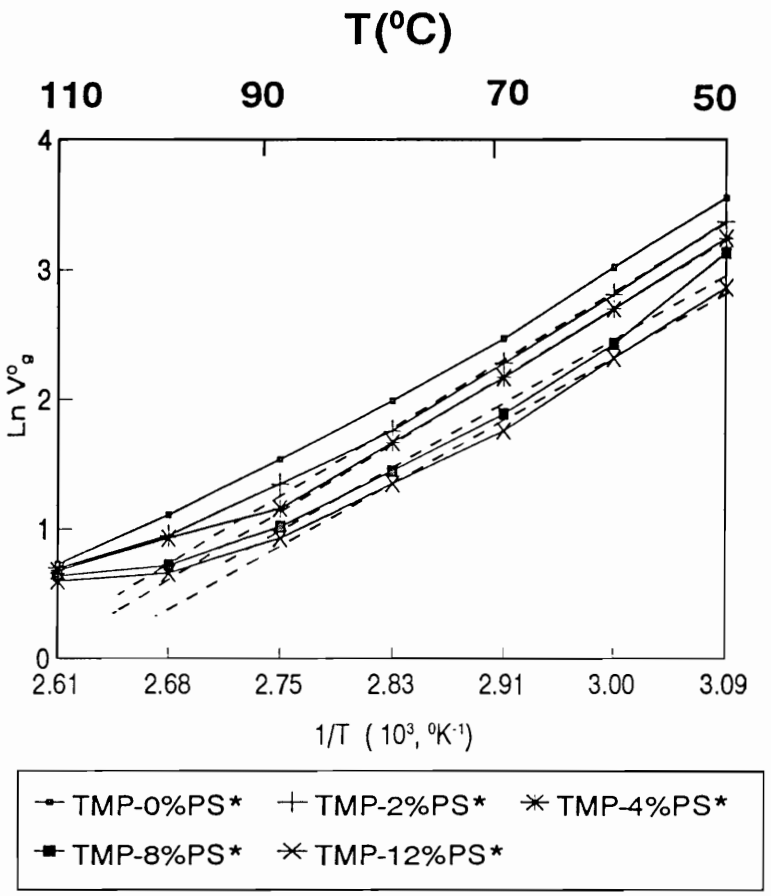

Figure 9. Retention diagram Ln V^0_g versus 1/T of n-decane on TMP-PS* samples.

5.2 Thermodynamics of Adsorption

5.2.1 *Standard free energy of adsorption*

The standard free energy of adsorption, ΔG^0_A, is the energy for the isothermal transfer of 1 mole of adsorbate (probe) from a reference standard gas pressure, $P_{s.g}$, to an adsorbed state (26). It was determined according to equation (6). The results of the three PS coated substrates at 60^{0}C are included in **Table 5**. The values of ΔG^0_A for all samples vary linearly with the number of carbon atoms for n-alkanes, as shown in **Figures 10, 11** and **12**. The slope of ΔG^0_A versus the number of carbon atoms is the free energy of adsorption of an incremental methylene group, $\Delta G^0_A(CH_2)$, which will be used to determine the London component of surface free energy (γ^L_S). $\Delta G^0_A(CH_2)$ is independent of the surface area of the adsorbent and can reflect only the interaction of the probe and the surface molecules of the adsorbent. The observed values of $\Delta G^0_A(CH_2)$ are shown in **Table 5**. For polystyrene coated TMP (TMP-PS*) composites, bulk TMP fiber (TMP-0%PS*) shows the highest negative value, indicating high interaction between probe and bulk TMP surface. The interaction decreases with the extent of PS* coating until 8%. For the CW-PS composites, bulk CW (CW-0%PS) has the lowest value, suggesting a weak interaction of probe and bulk CW. The value of $\Delta G^0_A(CH_2)$ becomes constant at 8% PS loading, implying that further

loading of PS will not change the interaction between the probe and the stationary phase. In contrast to the TMP-PS samples, CW-PS samples show increasing value of $\Delta G^0_A(CH_2)$ with the extent of PS loading, resulting from the different types of PS coated on CW surfaces. Bulk T14 sample (T14-0%PS) has a higher $\Delta G^0_A(CH_2)$ than either bulk TMP or CW substrate samples. This indicates the different nature of its surface.

5.2.2 *Standard enthalpy of adsorption*

The standard enthalpy of adsorption, ΔH^0_A, is calculated by using equation (8). At zero coverage, the adsorbate-adsorbate interaction is negligible and the standard enthalpy, ΔH^0_A, is identical to the heat of adsorption, q_d. The results of all samples at 60°C are tabulated in **Table 6**. **Figure 13** shows a linear variation of ΔH^0_A with the number of carbon atoms for TMP-PS* samples. The linearity indicates a flat orientation of the n-alkanes on the sample surface (25,27,35). The heats of liquefaction, ΔH_L, of n-octane, n-nonane, n-decane and n-undecane are 41.82, 46.81, 51.77 and 56.8 KJ·mole^{-1} at 20°C (27,30). The heat of liquefaction should be compared with the isosteric heat of adsorption (30). The isosteric heat of adsorption, q_{st}, is given by $q_{st} = q_d + RT$. At 60°C, RT is 2.77 KJ/mole. The values of q_{st} for n-decane are presented in **Table 7**. Compared to the ΔH_L, the isosteric

Table 5. Standard free energy ΔG^0_A at 60^0C.

Column	$-\Delta G^0_A$ (KJ/mole)					$\Delta G^0_A(CH_2)$ (KJ/mole)
	C_8H_{18}	C_9H_{20}	$C_{10}H_{22}$	$C_{11}H_{24}$	$C_{12}H_{26}$	
TMP-0%PS*	16.87	19.36	21.85	24.36	----	2.50
TMP-2%PS*	19.16	21.65	24.14	26.64	----	2.49
TMP-4%PS*	13.96	16.40	18.88	21.40	----	2.47
TMP-8%PS*	16.09	18.44	20.93	23.37	----	2.43
TMP-12%PS*	14.93	17.30	19.64	22.09	----	2.38
TMP-20%PS*	15.75	18.05	20.42	22.86	----	2.37
CW-0%PS	12.99	15.42	17.73	20.05	22.36	2.34
CW-2%PS	13.53	15.88	18.26	20.62	22.99	2.36
CW-4%PS	11.62	13.92	16.33	18.71	21.11	2.38
CW-8%PS	15.05	17.53	19.96	22.36	24.79	2.43
CW-12%PS	9.72	12.26	14.59	16.99	19.44	2.43
T14-0%PS	15.4	17.98	20.47	22.92	25.33	2.48
T14-2%PS	11.99	14.70	17.25	19.83	22.41	2.60
T14-4%PS	6.69	9.56	12.46	15.17	17.70	2.76
T14-8%PS	10.15	13.13	13.12	19.19	22.09	2.99
T14-12%PS	6.93	9.67	12.81	16.31	19.76	3.23
T14-20%PS	----	----	----	----	----	2.87

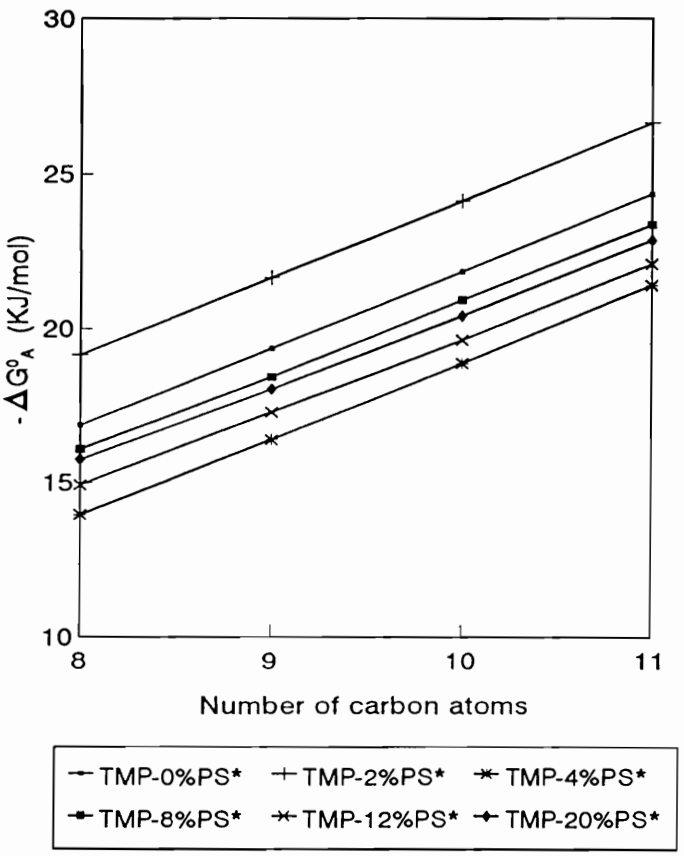

Figure 10. Linear variation of ΔG^0_A with probe size for TMP-PS* samples at 60^0C.

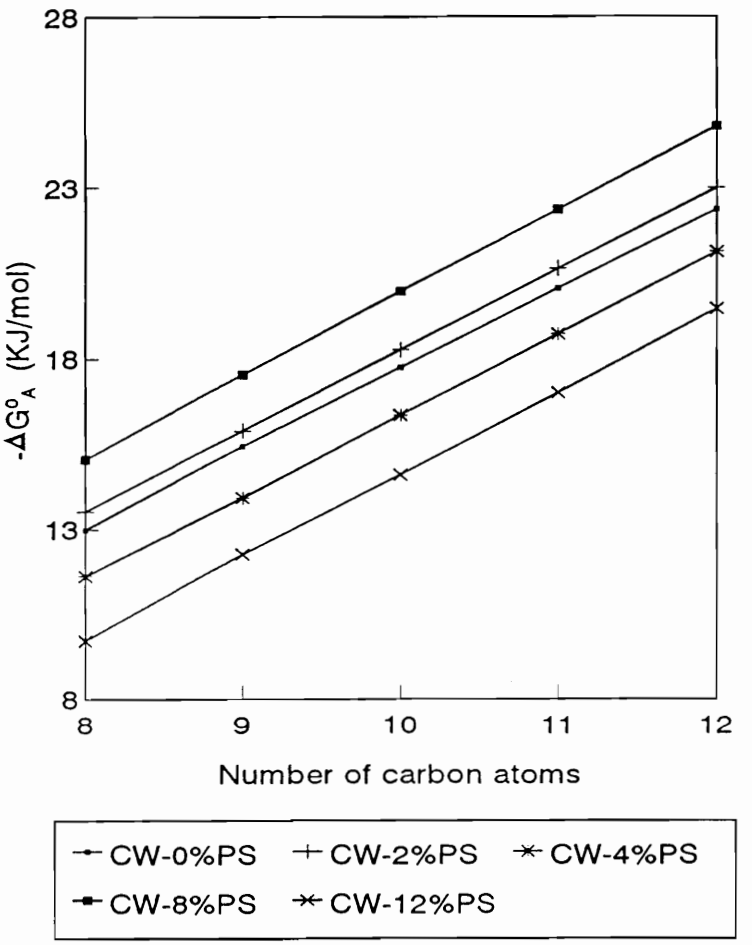

Figure 11. Linear variation of ΔG^0_A with probe size for CW-PS samples at 60^0C.

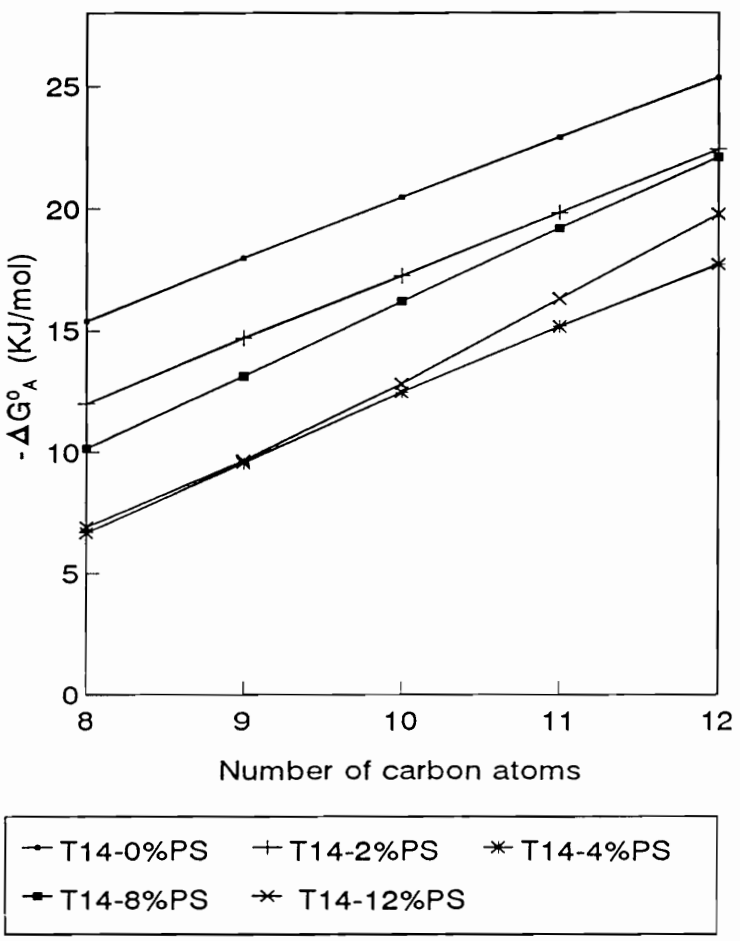

Figure 12. Linear variation of ΔG^0_A with probe size for T14-PS samples at 60^0C.

heats of adsorption, q_{St}, for the TMP-PS* composites are very close, indicating absence of high energy sites on the surfaces (30). Similar results were observed for CW-PS and T14-PS samples. **Table 6** shows that the bulk substrate CW (CW-0%PS) has higher ΔH^0_A values than the rest of the CW-PS samples due to the PS coverage on the solid substrates. Similar results were obtained for T14-PS . These results might imply that the surfaces of bulk CW and T14 substrates are more diverse than the PS surface. Compared to CW-PS and TMP-PS* samples, T14-PS samples show relatively lower q_d, especially for T14-12%PS and T14-20%PS samples. This may relate to a different PS configuration on the T14 substrates.

The value of q_d indicates the adsorption potential of the probe on the sample. It is, however, dependent on the nature of the stationary phase and the concentration of vapor probe injected (27,36). The surface structures of the PS coated substrates are very complex. The values of q_d in **Table 6** are rather scattered, and the change of q_d with the extent of PS loading appears to be random for the TMP-PS* composites. No significant trend is observed.

From the data in **Table 5** and **6**, it is shown that ΔG^0_A and ΔH^0_A are linearly related for n-alkanes on all samples. The consistent increment per CH_2 in the enthalpy of adsorption, is consistent with a flat orientation of the isolated n-alkane molecules on the surfaces of wood fibers

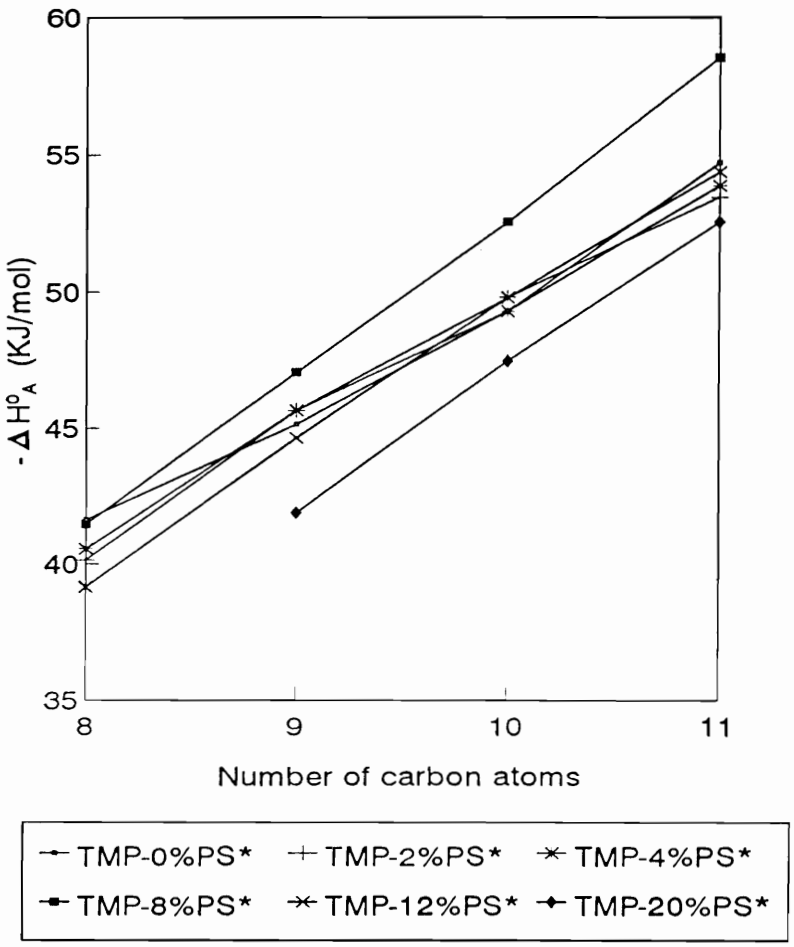

Figure 13. Variation of ΔH^0_A with probe size for TMP-PS* samples.

Table 6. Standard enthalpy of adsorption ΔH^0_A at 60^0C.

Column	$-\Delta H^0_A$ (KJ/mole)				
	C_8H_{18}	C_9H_{20}	$C_{10}H_{22}$	$C_{11}H_{24}$	$C_{12}H_{26}$
TMP-0%PS*	41.65	45.15	49.30	54.71	----
TMP-2%PS*	40.16	45.65	49.80	53.46	----
TMP-4%PS*	40.57	45.65	49.30	53.88	----
TMP-8%PS*	41.49	47.06	52.55	58.53	----
TMP-12%PS*	39.16	44.65	49.80	54.38	----
TMP-20%PS*	----	41.90	47.47	52.55	----
CW-0%PS	49.43	52.17	57.59	60.49	67.21
CW-2%PS	40.75	44.67	50.22	54.63	58.53
CW-4%PS	36.51	42.82	47.78	52.38	57.73
CW-8%PS	37.29	42.82	47.61	50.91	55.32
CW-12%PS	35.29	40.56	45.17	50.15	55.32
T14-0%PS	34.31	39.67	45.37	51.12	56.25
T14-2%PS	30.42	35.39	40.57	44.82	51.27
T14-4%PS	26.54	32.08	37.77	44.05	50.90
T14-8%PS	27.45	29.68	35.59	44.23	51.29
T14-12%PS	25.69	29.52	32.45	38.00	49.47
TMP-20%PS	-----	37.88	36.95	44.34	53.58

and Chromosorb W since this orientation permits the maximum number of contacts with a surface (26).

5.2.3 *Standard entropy of adsorption*

The entropy of adsorption, ΔS^0_A, of n-alkanes on various samples at 60^0C are obtained according to equation (8). The results are presented in **Table 8**. For TMP-PS* composites, no trend was observed. For CW-PS samples, bulk Chromosorb (CW-0%PS) displays the highest value of ΔS^0_A, suggesting that the surface of pure CW is more heterogeneous than others. The high (more negative) value of ΔS^0_A could be related to the loss of translational degrees of freedom in the adsorption process (26). Thus the adsorbed probe molecule is more restricted on the surface of pure CW. For TMP-PS* and T14-PS samples, the difference of ΔS^0_A among the bulk substrates and various PS coated samples is small.

5.2.4 *London component of surface free energy*

The slope of plots of ΔG^0_A versus the number of carbon atoms in the probe yields the free energy of adsorption of a single methylene unit, $\Delta G^0_A(CH_2)$, according to equation (13). This free energy then can be converted to the London component of the surface free energy, γ^L_s, via equation (12). This parameter is a significant measure of the London

Table 7. Standard thermodynamic functions for adsorption of $C_{10}H_{22}$ at 60^0C.

Column	q_d	ΔH_L	q_{st}
	(KJ/mole)		
TMP-0%PS*	49.30	51.77	52.07
TMP-2%PS*	49.80	51.77	52.57
TMP-4%PS*	49.30	51.77	52.07
TMP-8%PS*	52.55	51.77	55.32
TMP-12%PS*	49.80	51.77	52.57
TMP-20%PS*	47.47	51.77	50.54
CW-0%PS	57.59	51.77	60.39
CW-2%PS	50.22	51.77	52.99
CW-4%PS	47.78	51.77	50.55
CW-8%PS	47.61	51.77	50.38
CW-12%PS	45.17	51.77	47.94
T14-0%PS	45.37	51.77	48.14
T14-2%PS	40.57	51.77	43.34
T14-4%PS	37.77	51.77	40.54
T14-8%PS	35.59	51.77	38.36
T14-12%PS	32.45	51.77	35.22
T14-20%PS	36.95	51.77	39.72

Table 8. Standard entropy of adsorption ΔS^0_A at 60^0C.

	$-\Delta S^0_A$ (J/mole)				
Column	C_8H_{18}	C_9H_{20}	$C_{10}H_{22}$	$C_{11}H_{24}$	$C_{12}H_{26}$
TMP-0%PS*	74.40	77.43	82.38	91.09	----
TMP-2%PS*	63.03	72.04	77.03	80.50	----
TMP-4%PS*	79.88	87.79	91.31	97.50	----
TMP-8%PS*	76.23	85.91	94.92	105.55	----
TMP-12%PS*	72.72	82.08	90.53	96.92	----
TMP-20%PS*	----	71.61	81.20	89.12	----
CW-0%PS	109.37	110.3	119.66	121.39	134.63
CW-2%PS	81.69	86.44	95.94	102.09	106.68
CW-4%PS	74.71	86.74	94.42	101.03	109.93
CW-8%PS	66.74	75.90	82.99	85.69	91.63
CW-12%PS	76.98	85.24	91.79	99.55	107.71
T14-0%PS	56.77	65.09	74.75	84.64	92.80
T14-2%PS	55.33	62.11	70.00	75.01	86.62
T14-4%PS	59.59	67.61	75.97	86.69	99.67
T14-8%PS	51.96	49.72	58.15	75.18	87.67
T14-12%PS	56.33	59.51	58.95	65.10	89.18
T14-20%PS	----	----	----	----	----

forces which control the interaction of probe and substrate during the adsorption process. γ^L_S is dependent on the measurement temperature. **Table 9** gives the results for three composites at 60 and 70^{0}C. The plots of γ^L_S versus the PS loading are given in **Figure 14.** Bulk Chromosorb W (CW-0%PS) has the lowest γ^L_S for all the temperatures indicated. The γ^L_S increases with the extent of PS loading on the Chromosorb surface. The non-linear variation of γ^L_S with PS loading observed may be due to a non-homogenous composition of the surface. As the extent of PS increase above 8%, the γ^L_S becomes constant. This may suggest that interactions of the probe with the samples is mainly between the probe and the PS surface, and most of the CW surface is covered by PS above 8% PS loading. Thus interactions between probe and Chromosorb W become negligible beyond this point. Additional increments of PS on the Chromosorb will not change the surface properties, but only increase the thickness of the PS layer on CW surface. The surface properties of CW-PS samples with PS loading above 8% should approach that of a bulk PS sample.

The plots of γ^L_S versus the PS loadings for TMP-PS* composites are displayed in **Figure 15.** The bulk TMP sample (TMP-0%PS*) has the highest value of γ^L_S at all temperatures. γ^L_S is 34.28 $mN \cdot m^{-1}$ at 50^{0}C, 33.63 $mN \cdot m^{-1}$ at 60^{0}C, and 31.70 $mN \cdot m^{-1}$ at 70^{0}C. γ^L_S decreases with the amount of PS loading. The interactions between probe and TMP-PS*

composites might consist of three surfaces: bulk TMP fibers, bulk PS*, and the interface. Non-linear variation of γ^L_s with the percentage of PS loading is observed. The extent of the three components may not necessarily be a linear function of the percentage of PS in the composites. As the extent of PS on the wood substrate increases above 8%, γ^L_s becomes constant. This suggests that most of the TMP fiber surface is covered with PS. Additional increments of PS to the bulk matrix phase result in little or no change in the surface energy, γ^L_s.

γ^L_s was also obtained for T14-PS composites. The plots of γ^L_s versus PS loading are shown in **Figure 16**. A notable difference from both TMP-PS* and CW-PS samples is that the γ^L_s of T14-PS samples continues to increase even when the PS loading is above 8%. One possible explanation could be the larger specific surface area of T14 fiber. The relative specific surface area of T14 fiber to TMP fiber is approximately 1.25. A larger specific surface area could require more PS to cover the T14 surface. Another reason is possibly related to the treatment of T14 fiber by toluene. T14 fiber had been immersed in toluene for 12 hours, then the toluene was filtered away. Some wood extractive component might be removed from the fiber surface, pores and voids. The removal of wood extractives could contribute to the increase of pore and void dimensions, which lead to more PS penetration into the

Table 9. London component of free energy γ^L_s for the three substrates at 60 and 70°C.

Column	γ^L_s (mN/m)	
	60°C	70°C
TMP-0%PS*	33.63	31.70
TMP-2%PS*	33.58	30.58
TMP-4%PS*	33.12	29.84
TMP-8%PS*	31.90	29.41
TMP-12%PS*	30.55	28.76
TMP-20%PS*	30.32	28.81
CW-0%PS	29.49	27.09
CW-2%PS	30.22	27.92
CW-4%PS	30.48	28.36
CW-8%PS	31.84	29.68
CW-12%PS	31.75	30.32
T14-0%PS	33.15	31.07
T14-2%PS	36.38	34.31
T14-4%PS	41.18	38.40
T14-8%PS	48.39	45.21
T14-12%PS	56.28	54.07
T14-20%PS	44.40	41.63

fiber pores and voids. The treatment could also create higher energy sites on T14 surfaces. When 20% PS was coated on the T14 surface, the value of γ^L_s came down. This suggests that the T14 surface was becoming covered by the PS, and the surface properties were approaching to those of the bulk PS matrix. A parallel result for PS coated White Pine wood flour is observed from the data obtained by Rials and coworkers in another laboratory (37). γ^L_s increases with the PS loadings up to 15% as shown in **Figure 17.**

Compared to CW-PS samples, T14-PS samples show much higher γ^L_s at the same percent of PS loading. It was expected that γ^L_s would be the same when both substrates are completely covered by the PS, for example, T14-20%PS and CW-12%PS. The observed discrepancy is probably due to a different configuration of PS on the different substrates. The presence of PS on the T14 fiber surface may possibly create a more heterogenous surface and higher energy sites on the surface, which could lead to the increased γ^L_s. The evidence from SEM (Scanning Electron Microscopy) shows that PS was uniformly coated on both T14 and CW surfaces, which eliminates the possibility that the uneven distribution of PS on the substrate surface results in a different γ^L_s.

While it is plausible that PS in the interphase has a different γ^L_s from bulk PS, there are other explanations for what was happening. One is that our assumption of no

absorption of probe into the T14-PS surface may be in error. If the PS , in the interphase, or in the bulk, is deposited from the solution with a different polymer configuration, the void volume or density of the T14-PS surfaces may be different from TMP-PS* and CW-PS surfaces and allow different amounts of penetration (absorption) of the probes. In the lower temperature region, the absorption-desorption process was expected to occur at slow rate. When the absorption occurred in the T14-PS samples, different probes may have different absorptivities and different depths of penetration due to different sizes of the probes . These differences could lead to a larger different ΔG^0_A between probes, which finally leads to a larger value of $\Delta G^0_A(CH_2)$. Since γ^L_S is a square function of $\Delta G^0_A(CH_2)$, small change of $\Delta G^0_A(CH_2)$ could result in a very different γ^L_S. The observed values of $\Delta G^0_A(CH_2)$ of T14-PS samples were a little larger than those of TMP-PS* and CW-PS samples (see **Table 5**). The values of γ^L_S of T14-PS samples turn out to be much larger than those of TMP-PS* and CW-PS samples.

Compared to other thermodynamic parameters, the London component of surface free energy, γ^L_S, better reflects the interfacial properties of the composites investigated. The data from Kamdem and Riedl (27) show that the 30% of PMMA (polymethylmethacrylate) coated CTMP has the highest value of q_d, 60% has the highest ΔS^0_A, and

50% has the highest γ^{L}_{s}. Similar inconsistencies were also observed in this experiment. Unlike other thermodynamic parameters, γ^{L}_{s} is independent of the specific surface area of the samples. Thus γ^{L}_{s} better describes the interfacial properties in wood-plastic composites.

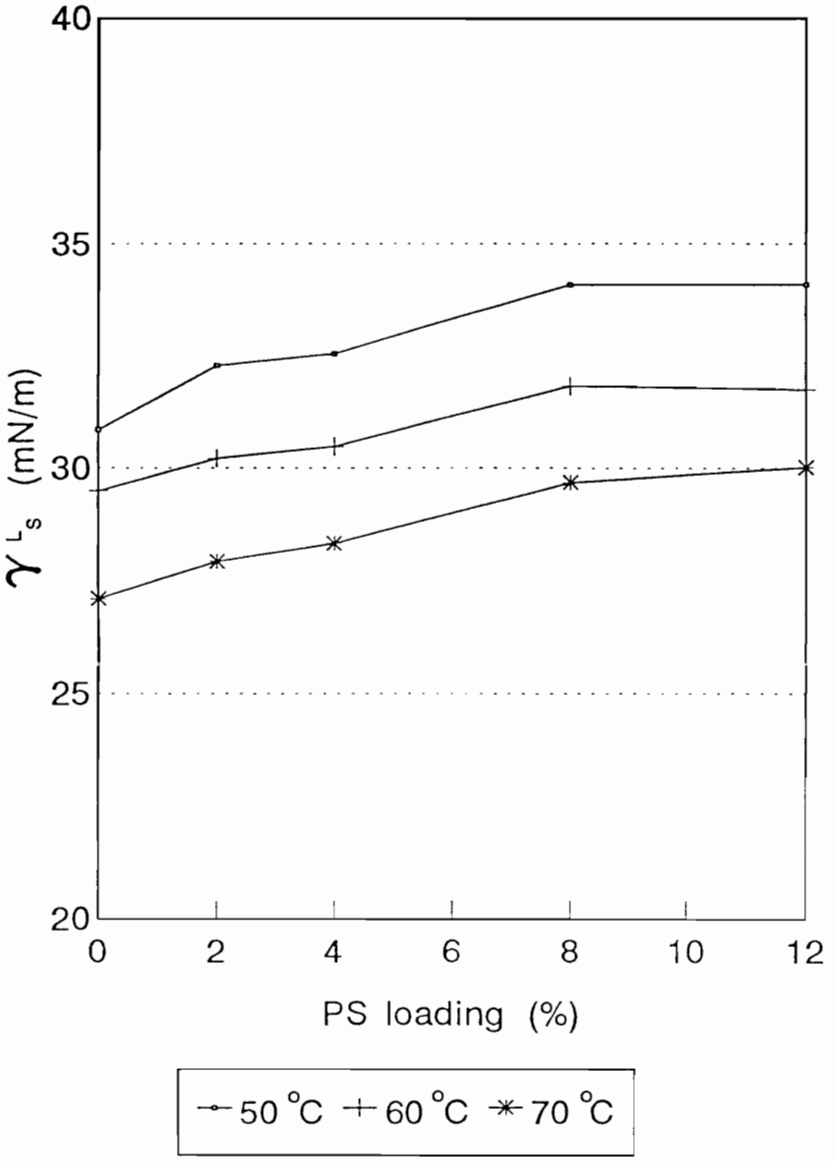

Figure 14. London component of free energy for CW-PS samples.

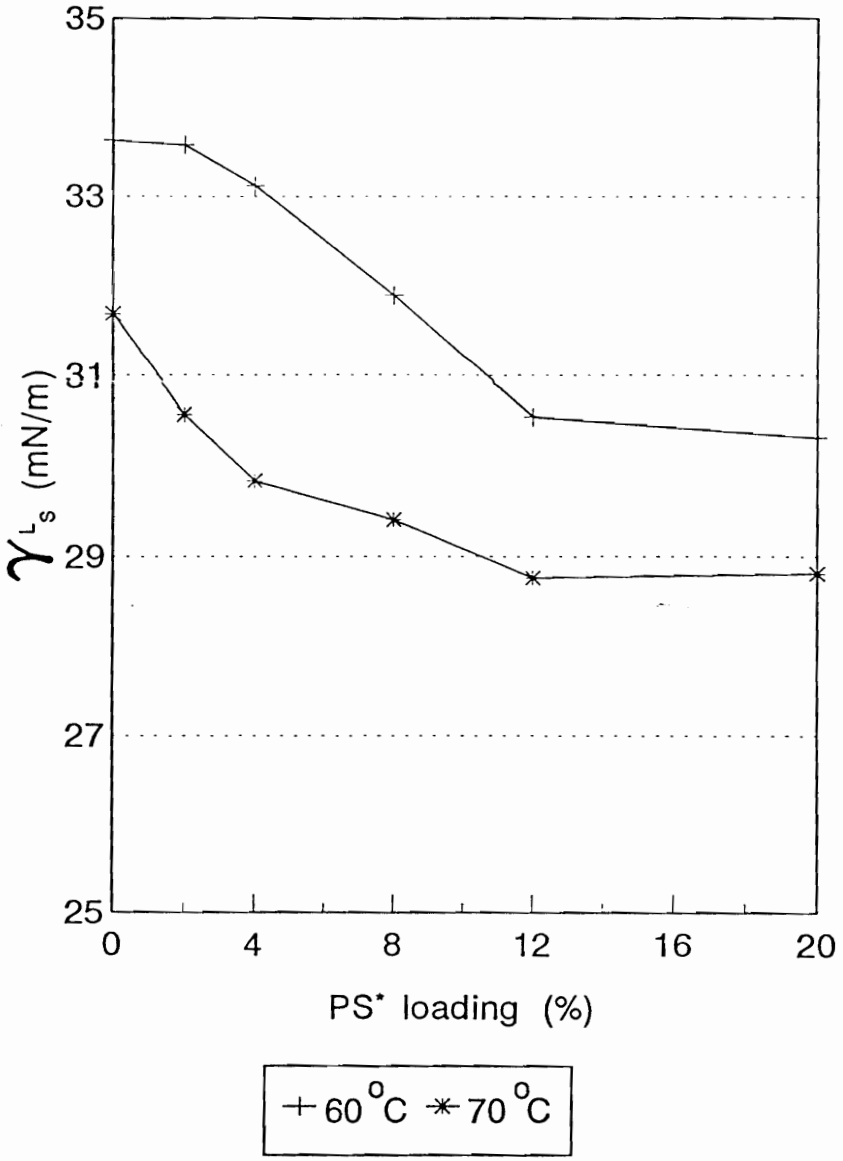

Figure 15. London component of free energy for TMP-PS* samples.

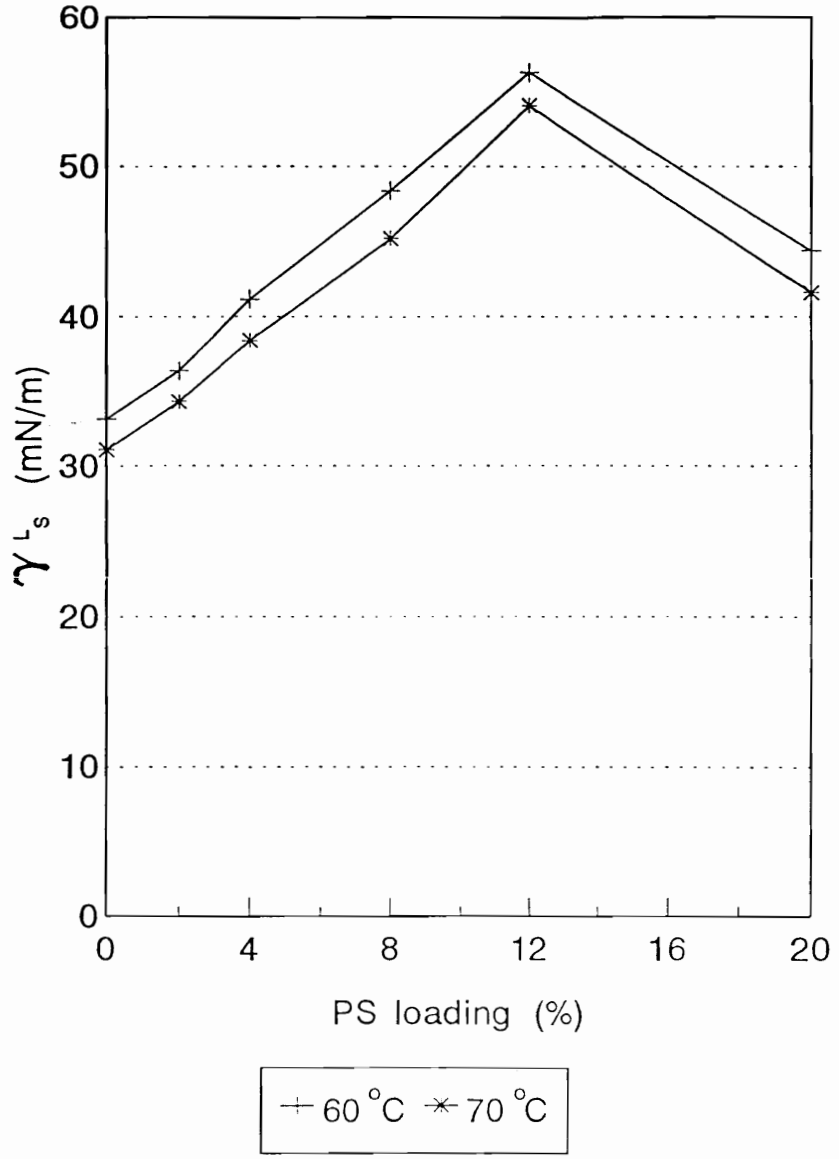

Figure 16. London component of free energy for T14-PS samples.

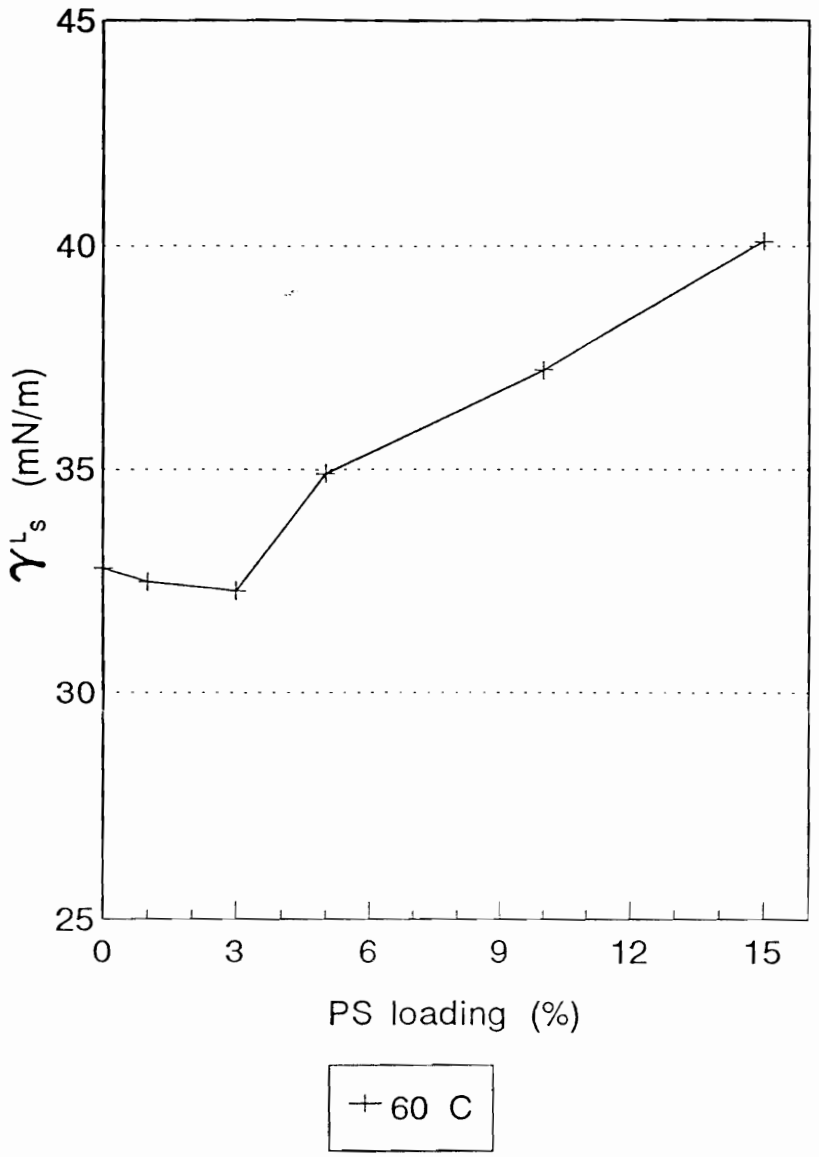

Figure 17. London component of free energy for White pine at 60^{0}C.

6. CONCLUSIONS

The results of this study confirm that the IGC technique is useful for the study of the interphase in wood-plastic composites. The information on adsorption volumes allows us to study the relationship between interfacial properties and composition in wood-plastic composites. The glass transition temperatures (T_g) were estimated using IGC. No other technique has achieved this in the interfacial region.

The thermodynamic functions, especially the London component of surface free energy (γ^L_s), obtained from the IGC technique are able to provide information on the interface properties in wood-plastic composites. The γ^L_s remained constant for PS coated TMP and Chromosorb W substrates when PS loadings exceed ca. 8% due to an uniform layer of PS built on the entire surface of TMP and Chromosorb W substrates. The γ^L_s of PS coated wood fiber T14 increased with the mass of PS loadings below 12%, and decreased sharply with a PS loading of 20%. This result suggests that more than 12% PS is needed to completely cover the T14 fiber surface. The different results observed with T14 suggest a distinct surface structures for T14 in comparison to TMP fibers. Inverse gas chromatography is able to determine the thermodynamic parameters of polymer coated substrates and provide information on the

interphase properties relating to the composition of wood-plastic composites.

7. LITERATURE CITED

1. Simonsen, J. and T. Rials. 1992. In Materials Interactions Relevant to Recycling of Wood-Based Materials. Rowell, R. M., T. L. Laufenberg and J. K. Rowell, ed., MRA Symposium Proceedings Vol. 26, Materials Research Society, Pittsburgh, Pennsylvania.

2. Maldas, L. and B. V. Kokta. 1991. Polym. Eng. Sci. **31**(18):1351-1357.

3. Yam, K. L., B. K. Gogoi, C. C. Lai and S. E. Selke. 1990. Polym. Eng. Sci. **30**(11):693-695.

4. Woodhams, R. T., G. Thomas and D. K. Rodgers. 1984. Polym. Eng. Sci. **24**(15):1165-1172.

5. Takase, S. and N. Shiraishi. 1989. J. Appl. Polym. Sci. **37**: 645-659.

6. Rowell, R. M., H. Spelter, R. A. Arola, P. Davis, T. Friberg, R. W. Hemingway, T. Rials, D. Luneke, R. Narayan, J. Simonsen and D. White. 1993. Forest Products Journal. **43** (1):55-63.

7. Kishi, H., M. Yoshioka, A. Yamanoi and N. Shiraishi. 1988. Mokuzai Gakkaishi. **34**(2):133-139.

8. Maldas, D., V. Kokta and C. Daneault. 1989. J. Appl. Polym. Sci. **37**:751-775.

9. Hon, D. N.-S. and W. Y. Chao. 1993. J. Appl. Polym. Sci. **50**:7-11.

10. Maldas, D and B. V. kokta. 1989. J. Adhesion Sci. Technol. **3**(7):529-539.

11. Han, G., H. Ichinose, S. Takase and N. Shiraishi. 1989. Mokuzai Gakkaishi. **35**(12):1100-1104.

12. Han, G. and N. Shiraishi. 1991. Mokuzai Gakkaishi. **37**(1):39-43.

13. Felix, J., P. Gatenholm, and H. P. Schreiber. 1994. J. Appl. Polym. Sci. **51**:285-295.

14. Gutman, V. 1978. The Donor-Acceptor Approach to Molecular Interactions. Plenum Press, New York.

15. Braun, J. M. and J. E. Guillet. 1976. In Advances in

Polymer Science. **21**:107-145. Springer-Verlag.

16. Schreiber, H. P. and D. R. Lloyd. 1989. In Inverse Gas Chromatography. Lloyd, D. R., T. C. Ward and H. P. Schreiber, ed., ACS symposium Series No. 391, American Chemical Society, Washington, DC.

17. Smidsrod, O. and J. E. Guillet. 1969. Macromolecules **2**:272-275.

18. Bolvari, A. E., T. C. Ward, P. A. Koning and D. P. Sheehy. 1989. In Inverse Gas Chromatography. Lloyd, D. R., T. C. Ward and H. P. Schreiber, ed., ACS symposium Series No. 391, American Chemical Society, Washington, DC.

19. Miller, J. M. 1988. Chromatography: Concepts and Contrasts. Wiley, New York.

20. Schultz, J. and L. Lavielle, 1989. In Inverse Gas Chromatography. Lloyd, D. R., T. C. Ward and H. P. Schreiber, ed., ACS symposium Series No. 391, American Chemical Society, Washington, DC.

21. Guillet, J. E., M. Romansky, G. J. Price and R. van der Mark. 1989. In Inverse Gas Chromatography. Lloyd, D. R., T. C. Ward, and H. P. Schreiber. ed., ACS symposium Series No. 391, American Chemical Society, Washington, DC.

22. Demertzis, P. G. and M. G. Kontominas. 1989. In Inverse Gas Chromatography. Lloyd, D. R., T. C. Ward, and H. P. Schreiber, ed., ACS symposium Series No. 391, American Chemical Society, Washington, DC.

23. Conder, J. R. and C. L. Young. 1979. Physicochemical Measurement by Gas Chromatography. John Wiley & Sons, New York.

24. Braun J. B. and J. E. Guilet. 1975. Macromolecules. **8**(6):882-888.

25. Vukov, A. J. and D. G. Gray. 1989. In Inverse Gas Chromatography. Lloyd, D. R., T. C. Ward and H. P. Schreiber, ed., ACS symposium Series No. 391, American Chemical Society, Washington, DC.

26. Dorris, G. M. and D. G. Gray. 1980. J. Colloid Interf. Sci. **77**(2):353-362.

27. Kamdem, D. P. and B. Riedl. 1991. J. Wood Chem. Technol. **11**(1):57-91.

28. Lipson, J. E. and J. E. Guillet. 1982. In Development in Polymer Characterization. 3rd ed. Dawkins, J. V. ed., Applied Science Publishers, Barking. pp. 33-74.

29. Fowkes, F. M. 1965. Chemistry and Physics of Interfaces. American Chemical Society, Washington, DC.

30. Katz, S. and D. G. Gray. 1981. J. Colloid Interf. Sci. **82**(2):312-325.

31. Mohlin, U-B and D. G. Gray. 1974. J. Colloid and Interf. Sci. **47**(3):747-754.

32. Dorris, G. M. and D. G. Gray. 1979. J. Colloid Interf. Sci. **71**(1):93-106.

33. Gurnagul, N. and D. G. Gray. 1987. Can. J. Chem. **65**:1935-1939.

34. Klotz, S., H. Grater and H. J. Cantow. 1989. In Inverse Gas Chromatography. Lloyd, D. R., T. C. Ward and H. P. Schreiber, ed., ACS symposium Series No. 391, American Chemical Society, Washington, DC.

35. Dorris, G. M. and D. G. Gray. 1981. J. Phys. Chem. **85**(24): 3628-3635.

36. Gray, D. G. and J. E. Guillet. 1972. Macromolecules. **5**(3):316-321.

37. Rials, T. 1995. Private communication, June 20.